
Towards generalizing deep-audio fake detection networks

Konstantin Gasenzer*
High Performance Computing
and Analytics Lab,
Universität Bonn, Germany
k.gasenzer@uni-bonn.de

Moritz Wolter*
High Performance Computing
and Analytics Lab,
Universität Bonn, Germany
moritz.wolter@uni-bonn.de

Abstract

Today’s generative neural networks allow the creation of high-quality synthetic speech at scale. While we welcome the creative use of this new technology, we must also recognize the risks. As synthetic speech is abused for both monetary and identity theft, we require a broad set of deep fake identification tools. Furthermore, previous work reported a limited ability of deep classifiers to generalize to unseen audio generators. By leveraging the wavelet- packet and short-time Fourier transform, we train excellent lightweight detectors that generalize. We report improved results on an extension of the WaveFake dataset. To account for the rapid progress in the field, we additionally consider samples drawn from the novel Avocodo and BigVGAN networks.

1 Introduction

The advancement of generative machine learning enables digital creativity, for example, in the form of more immersive video games and movies. However, it also creates new digital ways to lie. The technology is abused for theft [3, 4, 2] and disinformation [33]. Scammers use audio fakes to apply for remote jobs illicitly [3]. Via the telephone, cloned voices are misused in attempts to trick unsuspecting family members and stage fake kidnappings [4]. Problems have also surfaced on large platforms. Recently artificially generated songs with voices from two well-known artists illicitly appeared on a large music streaming service [1]. The fake recordings had been created and published without the artist’s consent.

Furthermore, modern technology allows the auto-generation of complete newscasts, simplifying disinformation campaigns by malicious actors [33]. Such fabrications could threaten the integrity of our public discourse, mainly because generative models facilitate the production of fake media at scale.

Consequently, we must meet the advancements in generative machine learning with an abundant collection of automatic deep fake detection tools. To this end, this work explores the use of wavelet transforms for this purpose.

This paper makes the following contributions:

- We challenge the commonly held belief that deep networks do not generalize well on audio data [12], and show that deep networks indeed generalize well on unknown audio fakes. We observe excellent generalization to unseen generators for networks trained on Wavelet Packet Transform (WPT) and Short-Time Fourier Transform (STFT) inputs.
- We improve upon synthetic media-recognition results published for the WaveFake dataset [12].

*Both authors contributed equally to this work

- To ensure our detectors identify the newest generators, we extend the dataset proposed in [12] by adding the very recent text to speech synthesis networks. We include the standard and large BigVGAN [13] architecture as well as the Avocado [5] network.
- This paper, for the first time, studies the application of the Wavelet Packet Transform (WPT) for audio-deep fake detection tasks.

To preserve the anonymity of the review process, we will share our source code and the data-set extension once the review process is complete.

2 Related work

2.1 Generative Models

The Mel-Generative Adversarial Network (GAN) architecture [23] was an early GAN in the audio domain. It proposed to work with mel-scaled spectrograms as an intermediate representation. The evolution of generative models with intermediate mel-representations continues with the HiFi-GAN architecture [22]. Its generator contains multiple residual blocks. Its training procedure minimizes the L1 distance between ground truth and generated mel-spectrograms. Parallel wave gan [40] integrates the WaveNet [30] architecture and uses the STFT intermediate representation. Similarly, WaveGlow combines a WaveNet backbone with a flow-based Glow paradigm [21]. The aforementioned architectures are part of the WaveFake-dataset [12].

Novel Text to Speech (TTS) systems have appeared since the publication of the WaveFake dataset. [13] for example, trained the biggest vocoder to date. Additionally, their architecture shifts to periodic activation functions. The authors report excellent generalization properties. The parallelly developed Avocado-Network [5] aims to reduce artifacts by removing low-frequency bias.

We additionally include both architectures in our study.

2.2 Audiofake detection

The ability of generative machine learning to generate credible media samples led to an investigation into their automatic detection. [38], for example, devised generative content detectors for images and found that CNN-detectors initialized on ImageNet do allow the detection of many other CNN-based generators, even if trained on only a single generator. While the deep learning community has focused lots of attention on the image domain [38, 39, 16, 8, 26, 11, 12, 34, 9], audio-manipulation has been neglected so far [12].

In the audio-domain, [12] recently established a novel baseline. The data-set includes five different generative network architectures in nine sample sets. In addition to collecting the data, two baseline models are established.

Some related work studies the ASVspoof 2019 [25] and 2021 [37] challenges. [29] for example evaluates multiple randomly initialized architectures. Their experiments include a ResNet18, a transformer, and a Light Convolutional Neural Network (LCNN) architecture [24]. The LCNN-architecture introduces max feature maps. These maps split the channel dimension in two. The resulting map contains the elementwise maximum of both halves. In addition to ASVspoof 2019, the authors add more recent examples. Using a similar architecture that combines Convolutional Neural Network (CNN) with a gated recurrent unit [20]. RawNet2 works directly on raw waveforms. The authors call their model RawNet2. The model did not generalize well on the original WaveFake data set [12].

2.3 Frequency analysis in audio processing

Frequency representations have a long track record in audio processing. These representations are biologically motivated since the cochlea inside the human inner ear acts as a spectrum analyzer [17]. Most of the literature chooses to work with the STFT[37, 31], or DCT [32, 12]. After mapping the data to the frequency domain, the dimensionality is often reduced via a set of filter banks [32]. These can be linearly- or mel-spaced. Mel-spacing produces a high resolution in lower frequency ranges, where humans hear exceptionally well.

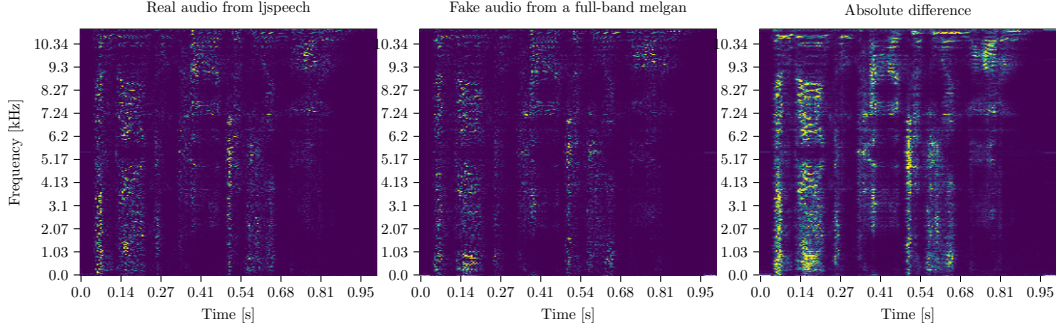


Figure 1: Wavelet packet visualizations of WaveFake [12] Sample LJ001-0002: "In being comparatively modern." A wavelet packet transformed version of the one-second long original recording is shown on the left. The center plot depicts a full-band melgan [23] re-synthesis. The plot on the right shows their absolute difference. As proposed by [16] for images, we normalize by dividing with the largest absolute coefficient from the real recording at each scale. The plots reveal differences across the board.

Like Mel-scaled STFT features, the Constant Q Transform (CQT) [36] is perceptually motivated. The approach delivers a higher frequency resolution for lower frequencies and a higher temporal resolution for higher frequencies [36]. The process is similar to the fast wavelet transform, which we will discuss next.

2.4 Wavelets in machine learning

Wavelets have a long track record in engineering and signal processing. More recently, wavelet methods have started to reappear in the artificial neural networks literature in the form of scatter-nets [27, 7], and synthetic image detection [39, 16, 26]. In the audio domain, [10] works with Mel spectrogram inputs and feed features from a standard wavelet tree in parallel to a traditional CNN at multiple scales. To the best of our knowledge, we are the first to explore direct training on wavelet packets as an alternative to Fourier or DCT features on audio.

3 Methods

High-frequency information was a crucial ingredient in previous work on images [11, 39]. Consequently, we explore wavelet packets and STFT as input representations. Both capture high-frequency information. Consider figure 1, for example. The figure considers a single utterance from the ljspeech data-set [18] and a full band melgan resynthesis. We observe differences for many frequencies. The next section discusses how to compute these wavelet packets.

3.1 The Fast Wavelet Transform (FWT)

The FWT works with two filter pairs. An analysis pair $\mathbf{h}_{\mathcal{L}}$, $\mathbf{h}_{\mathcal{H}}$ and a synthesis pair $\mathbf{f}_{\mathcal{L}}$, $\mathbf{f}_{\mathcal{H}}$. The analysis transform relies on convolutions with a stride of two. The first level of the transform computes

$$\mathbf{f}_{\mathcal{L}} *_{\downarrow 2} \mathbf{x} = \sum_k \mathbf{h}_{\mathcal{L}}[k] \mathbf{x}[n - k] = \mathbf{y}_a[n], \quad (1)$$

$$\mathbf{f}_{\mathcal{H}} *_{\downarrow 2} \mathbf{x} = \sum_k \mathbf{h}_{\mathcal{H}}[k] \mathbf{x}[n - k] = \mathbf{y}_d[n]. \quad (2)$$

Index k runs from 1 up to the filter length. Valid filter positions are indexed by n . $*_{\downarrow 2}$ symbolizes convolution with a stride of two. Padding is required to ensure every location is covered. Approximation coefficients have an a subindex. Detail coefficients use d . For the next level we compute $\mathbf{y}_{aa} = \mathbf{f}_{\mathcal{L}} *_{\downarrow 2} \mathbf{y}_a$ and $\mathbf{y}_{ad} = \mathbf{f}_{\mathcal{H}} *_{\downarrow 2} \mathbf{y}_a$. The process continues by recursively filtering the approximation coefficients. Introducing convolution matrices \mathbf{H} allows writing the analysis transform in matrix

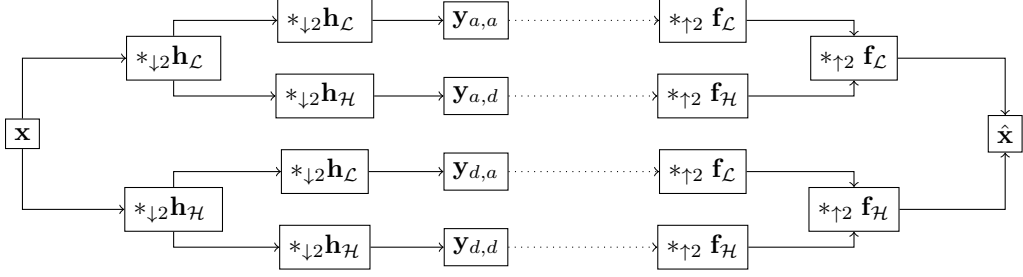


Figure 2: Visualisation of the wavelet packet transform. The figure uses \mathbf{h} to denote analysis filters, \mathbf{f} for synthesis filters, and stars $*$ for the convolution operation. The 0 subindex denotes lowpass- the 1 index denotes highpass-filters. $\downarrow 2$ denotes subsampling with a stride of two. $\uparrow 2$ denotes a transposed convolution with an upsampling effect and stride two. The notation follows [35]. The \mathbf{b} s denote the packet coefficients. The operation is invertible. Reconstruction produces an input-reconstruction $\hat{\mathbf{x}}$.

form [35],

$$\mathbf{A} = \dots \left(\begin{array}{c|c} \mathbf{H}_{\mathcal{L}} & \\ \mathbf{H}_{\mathcal{H}} & \\ \hline & \mathbf{I} \end{array} \right) \begin{pmatrix} \mathbf{H}_{\mathcal{L}} \\ \mathbf{H}_{\mathcal{H}} \end{pmatrix}. \quad (3)$$

the matrix structure illustrates how the process decomposes multiple scales. $\mathbf{H}_{\mathcal{L}}$ and $\mathbf{H}_{\mathcal{H}}$ denotes highpass and lowpass convolution matrices, respectively. Evaluating the matrix-product yields \mathbf{A} , the analysis matrix. In the factor matrices, the identity in the lower block grows with every scale. Therefore the process speeds up with every scale. The process is invertible. We could construct a synthesis matrix \mathbf{S} using transposed convolution matrices to undo the transform. See [35] or [19] for excellent in-depth discussions of the FWT.

3.2 Wavelet-packets

Related work [11, 39, 12, 34, 9] highlights the importance of high-frequency bands for detecting gan-generated images. Consequently, expanding only the low-frequency part of the discrete wavelet-transform will not suffice. Instead, we employ the wavelet packet transform [19]. To ensure a fine-grained frequency resolution, we expand the complete tree. This approach is also known as the Walsh-form [35] of the transform. Figure 2 illustrates the idea. The main idea is to recursively expand the tree in the low - and high-pass direction. We index tree nodes with the filter sequences. a denotes a low-pass or approximation, d a high-pass or detail step. Via full expansion, we improve the resolution in the relevant high-frequency part of the tree compared to the standard FWT. The full tree linearly subdivides the spectrum from zero until the Nyquist frequency at half the sampling rate.

Not all filters are suitable choices for the analysis and synthesis pairs. Appropriate choices must obey the perfect reconstruction and anti-aliasing conditions [35]. We found smaller Daubechies wavelets to be a good starting point. Symlets are a variant of the Daubechies-Wavelet family. Evaluating these symmetric cousins is usually the next step when exploring wavelet choices.

3.3 The Short-Time Fourier Transform (STFT)

By comparison, the STFT achieves localization in time via a sliding window. A sliding window \mathbf{w} segments the input prior to Fast Fourier Transform (FFT). Only the part where the window is non-zero is visible. Or formally [15]

$$\mathbf{X}[\omega, Sm] = \mathcal{F}(\mathbf{w}[Sm - l]\mathbf{x}[l]) = \sum_{l=-\infty}^{\infty} \mathbf{w}[Sm - l]\mathbf{x}[l]e^{-j\omega l}. \quad (4)$$

Here \mathcal{F} denotes the classic discrete FFT. S denotes the sampling period. We select specific windows with m , while ω denotes different frequencies in each window. In other words, after multiplying slices of \mathbf{x} with \mathbf{w} , the result is Fourier-transformed.

4 Training general detectors for synthetic audio

We ran our experiments on a four compute-node cluster with two Intel Xeon[®] Silver 4309Y 2,8GHz host CPUs and four A40 Nvidia graphics cards per host. All experiments require a single GPU. Our experimental work builds upon the Pytorch-Wavelet-Toolbox (ptwt) [28].

Figure 1 shows example plots normalized with the largest absolute value per scale. While this approach is well suited for human consumption, it did not help us when training artificial neural networks. In the following section we rescale by evaluating natural logarithm (ln) after computing the absolute value instead.

This experimental section studies the generalizing properties of deep fake-audio classifiers trained only on a single generator. We consider the wave fake data set [12] with all its generators, including the conformer-TTS samples and the Japanese language examples.

We add samples drawn from the Avocodo [5]. Due to a lack of pre-trained weights, we retrained using the publicly available implementation from [6] commit 2999557. We trained for 346 epochs or 563528 steps. Hyperparameters were chosen according to [5] with a learning rate of 0.0002 for the discriminator and generator. After training, we used their inference script to generate additional ljspeech samples.

Following a similar procedure, we add BigVGAN [13] generated audio files. We consider BigVGAN large (L) with 112M parameters, and it’s downsized counterpart with 14M weights, which we refer to as BigVGAN. We use the code from [14]. Again additional ljspeech fake samples are generated with the author’s inference script for both models.

The Japanese language (jsut) samples from [12] are downsampled from 24kHz to 22.050 kHz to ensure a sampling rate of 22.050 kHz for all generators. All samples are cut into one-second segments, with 22050 samples per segment. All sets contain an equal amount of real and fake samples. We use 111162 samples for training, 15862 for validation, and 31750 for testing.

4.1 Generalizing detectors for the extended WaveFake Dataset

This section studies the WaveFake dataset [12]. According to the measurements by [12] a Gaussian Mixture Model (GMM) trained on top of Linear Frequency Cepstral Coefficients (LFCCs) performed best on the original WaveFake dataset. [12] found the GMM outperformed a RawNet2 [20] architecture, which was trained on unmodified waveforms. Related work found high-frequency information a crucial component for fake-image detection. Motivated by these results, we explore the generalization of deep architectures on wavelet packets and STFT inputs. We adopt an LCNN-LSTM architecture [37] coupled with a cross-entropy loss. Adam trains all our networks using a learning rate of 0.0001. Each training step used 128 audio samples per batch. Finally, we employ weight decay. The L2 penalty is set to 0.01 unless stated otherwise.

Our input pipeline proceeds as follows; Audio is loaded first. After batching, we transform with either the WPT or STFT. Once the transformation is complete, we always take the absolute values of the result. We compare power one and power two spectra for all runs. Power two means we compute the square, power one means we do not. Generally, we compute the square and extra labels if we don’t. Finally, the result is ln-scaled. For the STFT, we feed this input into model the model.

The sign pattern is important for the WPT. Assume a wavelet-packet tensor \mathbf{P} , which is obtained by stacking the end nodes of the packet graph. Given the pattern of minus signs \mathbf{N} , we could invert the rescaling since $\exp(\ln(\text{abs}(\mathbf{P}))) \odot \mathbf{N} = \mathbf{P}$, if \odot denotes the Hadamard-product. Conserving the signs avoids information loss. For the WPT, we additionally explore two-channel inputs, where we tag on the sign pattern of the WPT. We call this case signed (SG).

Table 1 lists results on the extended WaveFake dataset. In addition to the generators described in [12], we add 13100 samples from Avocodo [5] and 26200 samples from two models of BigVGAN [13]. For the latter one, we utilize the base and large models and take the mean over both models. We re-synthesize all utterances in the LJSpeech corpus and obtain a total of 13100 audio files for Avocodo, 13100 BigVGAN, and 13100 for BigVGAN large. The table lists results on STFT features as well as signed and unsigned wavelet packets. Additionally, results of a retrained LFCC-GMM are listed. The LFCC-GMM performed best on the original dataset [12]. The performance of the packet transform depends on the choice of the wavelet. We start with a Daubechies-eight wavelet and its

Table 1: LCNN-LSTM source identification results on WaveFake [12] data set (with JSUT) combined with BigVGAN (L) and Avocodo. All input transforms work with 256-frequency bins. Our models are trained exclusively on samples drawn from a full-band-MelGAN. We report the test set accuracy and average Equal Error Rate (aEER). To add additional context, we report mean test set accuracy and aEER and standard deviation over five runs for all experiments using seeds 0 to 4. \ln denotes the natural logarithm. SG denotes signed log, p1 is power one spectrum (only absolute values).

Method	Accuracy [%]		aEER	
	max	$\mu \pm \sigma$	min	$\mu \pm \sigma$
LCNN-l \ln -STFT	94.81	93.84 \pm 0.85	0.059	0.068 \pm 0.008
LCNN-l \ln -STFT-p1	94.81	93.17 \pm 1.08	0.059	0.076 \pm 0.013
LCNN-l \ln -sym8	95.79	91.41 \pm 3.38	0.062	0.116 \pm 0.041
LCNN-l \ln -sym8-p1	96.54	94.53 \pm 2.47	0.047	0.080 \pm 0.036
LCNN-l \ln -db8	95.52	94.64 \pm 1.37	0.057	0.075 \pm 0.020
LCNN-l \ln -db8-p1	94.73	93.37 \pm 0.91	0.067	0.092 \pm 0.017
LCNN-l \ln -sym20	96.73	94.97 \pm 1.72	0.044	0.069 \pm 0.026
LCNN-l \ln -sym20-p1	97.22	94.82 \pm 2.67	0.038	0.072 \pm 0.038
LCNN-SG-l \ln -sym8	97.98	91.42 \pm 4.70	0.024	0.113 \pm 0.057
LCNN-SG-l \ln -sym8-p1	94.71	87.50 \pm 6.51	0.081	0.156 \pm 0.069
LCNN-SG-l \ln -db8	91.71	86.60 \pm 4.3	0.109	0.167 \pm 0.044
LCNN-SG-l \ln -db8-p1	91.54	88.43 \pm 2.28	0.119	0.151 \pm 0.024
LCNN-SG-l \ln -sym20	92.06	86.05 \pm 4.34	0.115	0.180 \pm 0.044
LCNN-SG-l \ln -sym20-p1	95.25	88.40 \pm 4.86	0.070	0.151 \pm 0.054
GMM-LFCC [12]	-	-	0.145	-

Table 2: Detection rates for our LCNN-LSTM using SG-l \ln -sym8-wavelet-packets on 256 bins for WaveFake as well as Avocodo, BigVGAN and Large-BigVGAN. We use a seed of 3 and evaluate on a test set containing equally distributed labels, including real audios. We consider a total of 17457 test files over 11 labels. We excluded JSUT and conformer samples.

Audio-Source	Accuracy [%]
Real	98.24
WaveFake	99.09
Avocodo	99.24
BigVGAN	98.61
L-BigVGAN	94.20

less asymmetrical sym8 variant. We observed an improved maximum accuracy and minimal Equal Error Rate (EER) in comparison to the STFT version. Including the packet’s sign pattern yields an additional boost for the sym8 wavelet. Our best-performing network uses the signed-sym8 input representation. Overall both STFT and WPT features allowed the LCNN to outperform the GMM approach from [12] on the extended dataset with 256 bins.

Table 2 lists detection rates for each source. Our sym8-wavelet-packets based-classifier manages to identify samples from both new and unknown sources correctly. While the L-BigVGAN samples are harder to detect, results are still on par with the performance we see on the WaveFake samples, which we deem acceptable.

We list the total number of optimizable parameters in Table 3. We find a modest increase in parameters in the signed scenario.

4.1.1 The original WaveFake dataset

We continue to study the original WaveFake [12] dataset in isolation. Table 4 enumerates the performance of our classifiers on this dataset. We find a different picture in comparison to Table 1. Excluding the newer BigVGAN and Avocodo networks shifts the observed performance in favor of

Table 3: Number of model parameters for all trained deep fake detectors.

Model	Freq. Bins	Filter length	Model Parameters
LCNN-ln-STFT	256	-	3,312,450
LCNN-ln-sym8	256	16	3,312,450
LCNN-ln-db8	256	16	3,312,450
LCNN-ln-sym20	256	40	3,312,450
LCNN-ln-STFT	512	-	12,758,850
LCNN-ln-sym8	512	16	12,758,850
LCNN-ln-db8	512	16	12,758,850
LCNN-ln-sym20	512	40	12,758,850
LCNN-SG-ln-sym8	256	16	3,314,050
LCNN-SG-ln-db8	256	16	3,314,050
LCNN-SG-ln-sym20	256	40	3,314,050

Table 4: Results on the original Wavefake-Dataset [12]. Again SG denotes signed-log experiments, and p1 the power one spectrum. Recall that the power one spectrum is computed by taking the absolute value function without a square. We cite baseline numbers as reported by [12]. All frequency representations work with 256 bins.

Method	WaveFake [12]			
	Accuracy [%]		aEER	
	max	$\mu \pm \sigma$	min	$\mu \pm \sigma$
LCNN-ln-STFT	99.52	99.38 \pm 0.11	0.002	0.005 \pm 0.002
LCNN-ln-STFT-p1	99.52	98.86 \pm 1.05	0.002	0.012 \pm 0.016
LCNN-ln-sym8	95.77	91.02 \pm 3.69	0.063	0.122 \pm 0.045
LCNN-ln-sym8-p1	97.00	94.92 \pm 2.16	0.045	0.076 \pm 0.035
LCNN-ln-db8	95.34	94.21 \pm 1.76	0.059	0.081 \pm 0.025
LCNN-ln-db8-p1	94.48	93.00 \pm 1.17	0.069	0.097 \pm 0.020
LCNN-ln-sym20	97.70	95.99 \pm 1.38	0.030	0.056 \pm 0.022
LCNN-ln-sym20-p1	97.93	95.89 \pm 2.21	0.028	0.06 \pm 0.037
LCNN-SG-ln-sym8	98.25	92.49 \pm 4.21	0.022	0.095 \pm 0.047
LCNN-SG-ln-sym8-p1	94.9	88.48 \pm 5.18	0.082	0.141 \pm 0.050
LCNN-SG-ln-db8	90.75	87.42 \pm 3.47	0.117	0.151 \pm 0.030
LCNN-SG-ln-db8-p1	91.87	88.42 \pm 2.06	0.109	0.143 \pm 0.020
LCNN-SG-ln-sym20	92.22	88.00 \pm 3.69	0.108	0.151 \pm 0.035
LCNN-SG-ln-sym20-p1	96.77	89.97 \pm 4.48	0.046	0.125 \pm 0.048
GMM-LFCC [12]	-	-	0.062	-
RawNet2 [12]	-	-	0.363	-

Table 5: Results on BigVGAN [13] and Avocodo[5]. Once more, SG denotes the an additional sign input channel, and p1 indicates a power one spectrum (only absolute values). For consistency with Tables 1 and 4, all transforms use 256 frequency bins.

Method	Avocodo				BigVGAN (L)				
	Accuracy [%]		aEER		Accuracy [%]		aEER		
	max	$\mu \pm \sigma$	min	$\mu \pm \sigma$	max	$\mu \pm \sigma$	min	$\mu \pm \sigma$	
STFT	99.62	99.55 \pm 0.09	0.000	0.001 \pm 0.002	72.30	66.08 \pm 4.95	0.333	0.386 \pm 0.042	
STFT-p1	99.62	99.54 \pm 0.10	0.000	0.001 \pm 0.002	71.45	64.38 \pm 5.03	0.342	0.400 \pm 0.040	
LCNN-LSTM-ln	sym8	99.35	98.93 \pm 0.51	0.004	0.012 \pm 0.01	94.42	89.44 \pm 3.94	0.082	0.143 \pm 0.045
	sym8-p1	99.29	97.64 \pm 2.34	0.004	0.035 \pm 0.042	95.17	91.26 \pm 5.35	0.071	0.123 \pm 0.061
	db8	99.10	97.94 \pm 0.76	0.007	0.027 \pm 0.014	96.12	94.93 \pm 0.97	0.055	0.073 \pm 0.017
	db8-p1	98.60	96.66 \pm 1.79	0.019	0.053 \pm 0.032	94.90	93.38 \pm 1.12	0.063	0.092 \pm 0.020
	sym20	99.47	97.02 \pm 3.26	0.002	0.043 \pm 0.054	92.47	89.35 \pm 3.36	0.110	0.145 \pm 0.039
	sym20-p1	99.27	98.66 \pm 0.50	0.005	0.018 \pm 0.010	93.95	88.08 \pm 6.26	0.089	0.153 \pm 0.065
	SG-sym8	97.99	92.38 \pm 3.59	0.017	0.118 \pm 0.061	96.74	86.11 \pm 8.81	0.040	0.191 \pm 0.112
	SG-sym8-p1	96.12	88.11 \pm 7.87	0.044	0.166 \pm 0.104	96.39	82.75 \pm 12.34	0.044	0.219 \pm 0.141
	SG-db8	95.94	89.54 \pm 4.99	0.062	0.153 \pm 0.078	93.94	81.46 \pm 8.46	0.095	0.246 \pm 0.101
	SG-db8-p1	95.73	92.91 \pm 1.6	0.071	0.115 \pm 0.025	91.19	86.22 \pm 4.78	0.142	0.204 \pm 0.058
SG-sym20	94.87	86.91 \pm 6.13	0.086	0.196 \pm 0.077	89.91	76.83 \pm 8.43	0.160	0.301 \pm 0.085	
SG-sym20-p1	96.93	90.73 \pm 5.87	0.050	0.141 \pm 0.081	88.54	80.13 \pm 7.82	0.175	0.270 \pm 0.081	
GMM-LFCC [12]	-	-	0.316	-	-	-	0.432	-	

Table 6: LCNN-LSTM source identification results on WaveFake data set (with JSUT) combined with BigVGAN (L) and Avocodo. All models are trained on the subdataset of FB-MelGAN. We report the test set accuracy and average Equal Error Rate (aEER). To add additional context, we report mean test set accuracy and aEER and standard deviation over five runs for all experiments using seeds 0 to 4. ln denotes the natural logarithm.

Method	Accuracy [%]		aEER	
	max	$\mu \pm \sigma$	min	$\mu \pm \sigma$
ln-STFT	97.71	87.15 \pm 18.35	0.030	0.137 \pm 0.180
ln-STFT-p1	97.28	90.70 \pm 7.24	0.038	0.114 \pm 0.083
ln-sym8	96.44	93.95 \pm 2.50	0.048	0.084 \pm 0.037
ln-sym8-p1	95.20	92.04 \pm 2.67	0.071	0.117 \pm 0.040
ln-db8	93.62	90.27 \pm 4.58	0.086	0.128 \pm 0.055
ln-db8-p1	93.16	92.59 \pm 0.79	0.092	0.100 \pm 0.010
ln-sym20-p1	95.22	93.37 \pm 1.21	0.069	0.095 \pm 0.017

the STFT for the 256-bin case. However, we note that all our networks beat the baseline established in [12] by a substantial margin.

4.1.2 BigVGAN [13] and Avocodo [5]

Please consider Table 5 to understand the root of the differences we previously observed in section 4.1.1. Table 5 reveals the performance of our classifiers when tasked to identify our most recent vocoders in isolation. Our STFT based networks struggle with identifying BigVGAN samples at a 256-bin resolution. The signed and unsigned WPT based networks do much better on this task.

4.1.3 Increasing the frequency resolution all transforms

We study the effect of an increased frequency resolution in Table 6 and leave all other parameters unchanged. Overall a higher resolution yields an improved network trained on the STFT. However, it also introduces instability into the training procedure. We observe higher standard deviations over multiple repetitions. The sym8 WPT network also benefits, but the effect is less pronounced compared to the STFT.

5 Conclusion

In this paper, we studied the WaveFake-dataset [12] and an extended version with two additional GANs. We found the WPT added value in a 256-frequency bin scenario. In other words, the WPT-features worked at lower resolutions. In high-resolution set-ups, the STFT performed better. Our findings suggest applications for WPT representations on audio-data at low sampling rates or in the presence of compression. We intend to explore these scenarios in future work. While [12] suggested the use of traditional methods to avoid overfitting to individual audio generators, our combined CNN-Long Short Term Memory (LSTM)-based classifiers generalize very well on two-dimensional frequency domain inputs. This result holds regardless of the representation we choose.

References

- [1] Ai song featuring fake drake and weeknd vocals pulled from streaming services. <https://www.theguardian.com/music/2023/apr/18/ai-song-featuring-fake-drake-and-weeknd-vocals-pulled-from-streaming-services>. Accessed: 2023-05-11.
- [2] Audio deepfake scams: Criminals are using ai to sound like family and people are falling for it. <https://www.euronews.com/next/2023/03/25/audio-deepfake-scams-criminals-are-using-ai-to-sound-like-family-and-people-are-falling-fo>. Accessed: 2023-05-11.
- [3] Fbi: Scammers are interviewing for remote jobs using deepfake tech. <https://www.pcmag.com/news/fbi-scammers-are-interviewing-for-remote-jobs-using-deepfake-tech>. Accessed: 2023-05-11.
- [4] ‘mom, these bad men have me’: She believes scammers cloned her daughter’s voice in a fake kidnapping. <https://edition.cnn.com/2023/04/29/us/ai-scam-calls-kidnapping-cec/index.html>. Accessed: 2023-05-11.
- [5] Taejun Bak, Junmo Lee, Hanbin Bae, Jinhyeok Yang, Jae-Sung Bae, and Young-Sun Joo. Avocado: Generative adversarial network for artifact-free vocoder. *arXiv preprint arXiv:2206.13404, accepted for publication at the 37th AAAI conference on artificial intelligence (to appear)*, 2022.
- [6] Taejun Bak, Junmo Lee, Hanbin Bae, Jinhyeok Yang, Jae-Sung Bae, and Young-Sun Joo. Github-repository - avocado: Generative adversarial network for artifact-free vocoder. <https://github.com/ncsoft/avocado/commit/2999557bbd040a6f3eb6f7006a317d89537b78cd>, 2023. Accessed: 2023-05-17.
- [7] Fergal Cotter. *Uses of complex wavelets in deep convolutional neural networks*. PhD thesis, University of Cambridge, 2020.
- [8] Shichao Dong, Jin Wang, Jiajun Liang, Haoqiang Fan, and Renhe Ji. Explaining deepfake detection by analysing image matching. In *Computer Vision–ECCV 2022: 17th European Conference, Tel Aviv, Israel, October 23–27, 2022, Proceedings, Part XIV*, pages 18–35. Springer, 2022.
- [9] Tarik Dzanic, Karan Shah, and Freddie Witherden. Fourier spectrum discrepancies in deep network generated images. *Advances in neural information processing systems*, 33:3022–3032, 2020.
- [10] Abderrahim Fathan, Jahangir Alam, and Woohyun Kang. Multiresolution decomposition analysis via wavelet transforms for audio deepfake detection. In *Speech and Computer: 24th International Conference, SPECOM 2022, Gurugram, India, November 14–16, 2022, Proceedings*, pages 188–200. Springer, 2022.
- [11] Joel Frank, Thorsten Eisenhofer, Lea Schönherr, Asja Fischer, Dorothea Kolossa, and Thorsten Holz. Leveraging frequency analysis for deep fake image recognition. In *International conference on machine learning*, pages 3247–3258. PMLR, 2020.
- [12] Joel Frank and Lea Schönherr. Wavefake: A data set to facilitate audio deepfake detection. In Joaquin Vanschoren and Sai-Kit Yeung, editors, *Proceedings of the Neural Information Processing Systems Track on Datasets and Benchmarks 1, NeurIPS Datasets and Benchmarks 2021, December 2021, virtual*, 2021.

- [13] Sang gil Lee, Wei Ping, Boris Ginsburg, Bryan Catanzaro, and Sung-Hoon Yoon. Bigvgan: A universal neural vocoder with large-scale training. *International Conference on Learning Representations (ICLR) 2023*, 2023.
- [14] Sang gil Lee, Wei Ping, Boris Ginsburg, Bryan Catanzaro, and Sungroh Yoon. Github-repository - bigvgan: A universal neural vocoder with large-scale training. <https://github.com/nvidia/bigvgan>, 2023. Accessed: 2023-05-17.
- [15] Daniel Griffin and Jae Lim. Signal estimation from modified short-time fourier transform. *IEEE Transactions on acoustics, speech, and signal processing*, 32(2):236–243, 1984.
- [16] Wei Huang, Michelangelo Valsecchi, and Michael Multerer. Anisotropic multiresolution analyses for deep fake detection. *arXiv preprint arXiv:2210.14874*, 2022.
- [17] Xuedong Huang, Alex Acero, Hsiao-Wuen Hon, and Raj Reddy. *Spoken language processing: A guide to theory, algorithm, and system development*. Prentice hall PTR, 2001.
- [18] Keith Ito and Linda Johnson. The lj speech dataset. <https://keithito.com/LJ-Speech-Dataset/>, 2017.
- [19] Arne Jensen and Anders la Cour-Harbo. *Ripples in mathematics: the discrete wavelet transform*. Springer Science & Business Media, 2001.
- [20] Jee-weon Jung, Seung-bin Kim, Hye-jin Shim, Ju-ho Kim, and Ha-Jin Yu. Improved rawnet with feature map scaling for text-independent speaker verification using raw waveforms. In Helen Meng, Bo Xu, and Thomas Fang Zheng, editors, *Interspeech 2020, 21st Annual Conference of the International Speech Communication Association, Virtual Event, Shanghai, China, 25-29 October 2020*, pages 1496–1500. ISCA, 2020.
- [21] Durk P Kingma and Prafulla Dhariwal. Glow: Generative flow with invertible 1x1 convolutions. *Advances in neural information processing systems*, 31, 2018.
- [22] Jungil Kong, Jaehyeon Kim, and Jaekyoung Bae. Hifi-gan: Generative adversarial networks for efficient and high fidelity speech synthesis. *Advances in Neural Information Processing Systems*, 33:17022–17033, 2020.
- [23] Kundan Kumar, Rithesh Kumar, Thibault De Boissiere, Lucas Gestin, Wei Zhen Teoh, Jose Sotelo, Alexandre de Brébisson, Yoshua Bengio, and Aaron C Courville. Melgan: Generative adversarial networks for conditional waveform synthesis. *Advances in neural information processing systems*, 32, 2019.
- [24] Galina Lavrentyeva, Sergey Novoselov, Egor Malykh, Alexander Kozlov, Oleg Kudashev, and Vadim Shchemelinin. Audio Replay Attack Detection with Deep Learning Frameworks. In *Proc. Interspeech 2017*, pages 82–86, 2017.
- [25] Galina Lavrentyeva, Sergey Novoselov, Andzhukaev Tseren, Marina Volkova, Artem Gorlanov, and Alexandr Kozlov. STC antispooofing systems for the asvspoof2019 challenge. In Gernot Kubin and Zdravko Kacic, editors, *Interspeech 2019, 20th Annual Conference of the International Speech Communication Association, Graz, Austria, 15-19 September 2019*, pages 1033–1037. ISCA, 2019.
- [26] Jiaming Li, Hongtao Xie, Lingyun Yu, and Yongdong Zhang. Wavelet-enhanced weakly supervised local feature learning for face forgery detection. In *Proceedings of the 30th ACM International Conference on Multimedia*, pages 1299–1308, 2022.
- [27] Stéphane Mallat. Group invariant scattering. *Communications on Pure and Applied Mathematics*, 65(10):1331–1398, 2012.
- [28] Moritz Wolter. *Frequency Domain Methods in Recurrent Neural Networks for Sequential Data Processing*. PhD thesis, Rheinische Friedrich-Wilhelms-Universität Bonn, July 2021.
- [29] Nicolas M. Müller, Pavel Czempin, Franziska Dieckmann, Adam Froghyar, and Konstantin Böttinger. Does audio deepfake detection generalize? In Hanseok Ko and John H. L. Hansen, editors, *Interspeech 2022, 23rd Annual Conference of the International Speech Communication Association, Incheon, Korea, 18-22 September 2022*, pages 2783–2787. ISCA, 2022.
- [30] Aaron van den Oord, Sander Dieleman, Heiga Zen, Karen Simonyan, Oriol Vinyals, Alex Graves, Nal Kalchbrenner, Andrew Senior, and Koray Kavukcuoglu. Wavenet: A generative model for raw audio. *arXiv preprint arXiv:1609.03499*, 2016.

- [31] Kamalesh Palanisamy, Dipika Singhania, and Angela Yao. Rethinking cnn models for audio classification. *arXiv preprint arXiv:2007.11154*, 2020.
- [32] Md Sahidullah, Tomi Kinnunen, and Cemal Haniilçi. A comparison of features for synthetic speech detection. 2015.
- [33] Adam Satariano and Paul Mozur. The people onscreen are fake. the disinformation is real. <https://www.nytimes.com/2023/02/07/technology/artificial-intelligence-training-deepfake.html>. Accessed: 2023-05-11.
- [34] Katja Schwarz, Yiyi Liao, and Andreas Geiger. On the frequency bias of generative models. *Advances in Neural Information Processing Systems*, 34:18126–18136, 2021.
- [35] Gilbert Strang and Truong Nguyen. *Wavelets and filter banks*. SIAM, 1996.
- [36] Massimiliano Todisco, Héctor Delgado, and Nicholas WD Evans. A new feature for automatic speaker verification anti-spoofing: Constant q cepstral coefficients. In *Odyssey*, volume 2016, pages 283–290, 2016.
- [37] Anton Tomilov, Aleksei Svishchev, Marina Volkova, Artem Chirkovskiy, Alexander Kondratev, and Galina Lavrentyeva. STC Antispoofing Systems for the ASVspoof2021 Challenge. In *Proc. 2021 Edition of the Automatic Speaker Verification and Spoofing Countermeasures Challenge*, pages 61–67, 2021.
- [38] Sheng-Yu Wang, Oliver Wang, Richard Zhang, Andrew Owens, and Alexei A. Efros. Cnn-generated images are surprisingly easy to spot... for now. In *2020 IEEE/CVF Conference on Computer Vision and Pattern Recognition, CVPR 2020, Seattle, WA, USA, June 13-19, 2020*, pages 8692–8701. Computer Vision Foundation / IEEE, 2020.
- [39] Moritz Wolter, Felix Blanke, Raoul Heese, and Jochen Garcke. Wavelet-packets for deepfake image analysis and detection. *Machine Learning*, Special Issue of the ECML PKDD 2022 Journal Track:1–33, August 2022.
- [40] Ryuichi Yamamoto, Eunwoo Song, and Jae-Min Kim. Parallel wavegan: A fast waveform generation model based on generative adversarial networks with multi-resolution spectrogram. In *ICASSP 2020-2020 IEEE International Conference on Acoustics, Speech and Signal Processing (ICASSP)*, pages 6199–6203. IEEE, 2020.

Acronyms

CNN	Convolutional Neural Network
CQT	Constant Q Transform
EER	Equal Error Rate
FFT	Fast Fourier Transform
FWT	Fast Wavelet Transform
GAN	Generative Adversarial Network
GMM	Gaussian Mixture Model
LCNN	Light Convolutional Neural Network
LFCC	Linear Frequency Cepstral Coefficient
ln	natural logarithm
LSTM	Long Short Term Memory
STFT	Short-Time Fourier Transform
TTS	Text to Speech
WPT	Wavelet Packet Transform

6 Supplementary

Figure 3 depicts the mean of the largest absolute packet values along the time-axis. We see different frequency-domain patterns for all generators on the WaveFake core data, excluding the Japanese language samples.

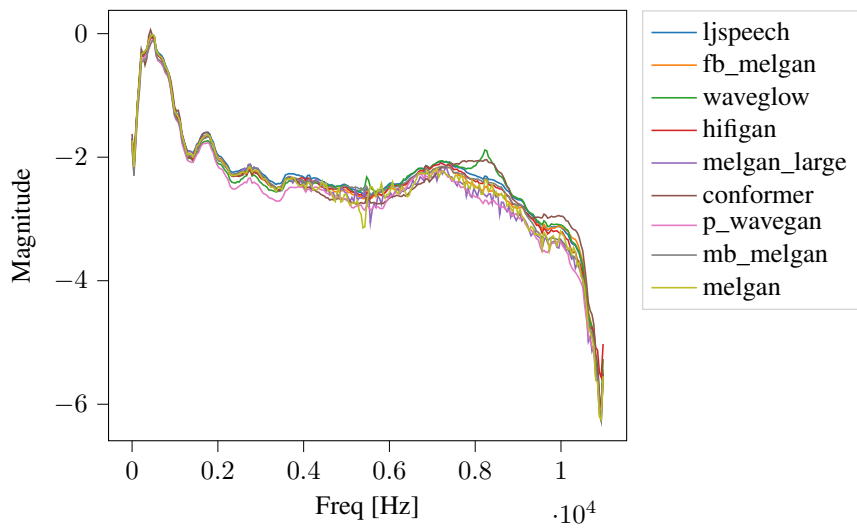


Figure 3: Comparison of the largest entries per frequency of various audio sources.